A novel flow chamber for biodegradable alloy assessment in physiologically realistic environments

J. A. Grogan[1], D. Gastaldi[2], M. Castelletti[2], F. Migliavacca[2], G. Dubini[2], P. E. McHugh[1]

[1] Mechanical and Biomedical Engineering, National University of Ireland, Galway

[2] Laboratory of Biological Structure Mechanics, Chemistry, Materials and Chemical Engineering "Giulio Natta" Department, Politecnico di Milano, Milano, Italy

Abstract

In order to better understand the *in-vivo* corrosion of biodegradable alloys it is necessary to replicate the physiological environment as closely as possible. In this study a novel flow chamber system is developed that allows the investigation of biodegradable alloy corrosion in a simulated physiological environment. The system is designed to reproduce flow conditions encountered in coronary arteries using a parallel plate setup and to allow the culturing of cells. Computational fluid dynamics and analytical methods are used as part of the design process to ensure that suitable flow conditions are maintained in the test region. The system is used to investigate the corrosion behaviour of AZ31 alloy foils of different thickness, in test media with and without proteins and in static and dynamic solutions. It is observed that pulsatile flows, similar to those in the coronary arteries, significantly increase corrosion rates and lead to a different corrosion surface morphologies relative to static immersion tests.

1. Introduction

Stents are commonly used to treat atherosclerosis by providing mechanical support to the artery vessels, preventing early recoil. Since remodelling of arterial vessels is expected, the role of stents should be temporary. However, current stent technology is based on permanent implants, which can eventually lead to long term complications.[1,2] In the last decade,

biodegradable materials have shown great potential in clinical applications and have become the focus of many researchers.[3-5] Metallic stents that will gradually dissolve in the body (eventually leaving no device behind), or biodegradable metal stents, have the potential to both provide initial scaffolding and avoid long term clinical problems.

Bearing in mind the complex and dynamic *in-vivo* corrosion environment, it is clear that the design of biodegradable implants brings a number of new challenges. Among these, the most relevant are difficulties in precisely and adequately controlling the device corrosion rate and in developing an adequate biodegradable alloy that is compatible with the vessel wall (endothelial and smooth muscle cells). Disparities between biodegradable magnesium alloy corrosion behaviour *in-vivo* and *in-vitro* have been reported in the literature,[6-8] which suggests that typical *in-vitro* tests may not fully capture transport conditions in the body. In order to obtain more reliable corrosion rates, the development of an appropriate *in-vitro* pseudo-physiological system, i.e. a bioreactor, which reflects as closely as possible the actual behaviour of the alloys in the arterial environment and simultaneously allows the control of different parameters such as shear stress, is of great interest.

The main goal of the present work is the design and application of a novel flow chamber that is able to reproduce a physiologically realistic environment for the evaluation of corrosion rates of biodegradable alloys in stent applications. In particular, the environment approximates physiological conditions encountered in coronary arteries and is amenable to the culturing of endothelial and smooth muscle cells, i.e. that of a bioreactor. In the first part of the present work, fluid dynamic conditions in the bioreactor are evaluated by means of analytical methods and computational fluid dynamics (CFD). It is verified that the flow regime in the bioreactor is laminar and that the shear stress exerted on alloy specimens is uniform and falls in the physiological range. In the second part, the bioreactor is used to

assess the corrosion behaviour of AZ31 magnesium alloy. The influence of alloy foil thickness, flow conditions and test media on corrosion behaviour is evaluated.

2. Materials and Methods

2.1 Bioreactor Design

The bioreactor system uses a parallel plate flow chamber (PPFC), which is similar to those used in cell culture studies,[9] but modified to also allow the study of biodegradable alloys. The system is designed with the requirements that:

- The mean wall shear stress (WSS) is between 1.5 and 2.0 Pa, corresponding to physiological values in the arteries.[10]
- An active test region (ATR) can be identified in the chamber where flow is fully developed and where the WSS is uniform and constant along the length.
- The ATR is of sufficient length to allow six samples to be tested concurrently.
- The flow is laminar.
- Samples with planar geometry can be used, to facilitate cell culture and microscopy.
- The system can be used to culture cells and is sufficiently compact to fit in an incubator.

A schematic of the bioreactor system is shown in Fig. 1 (a). It consists of a peristaltic pump, which delivers a pulsatile flow, an open reservoir containing 500 ml of test media and the PPFC. During testing the reservoir is maintained at 37 °C.

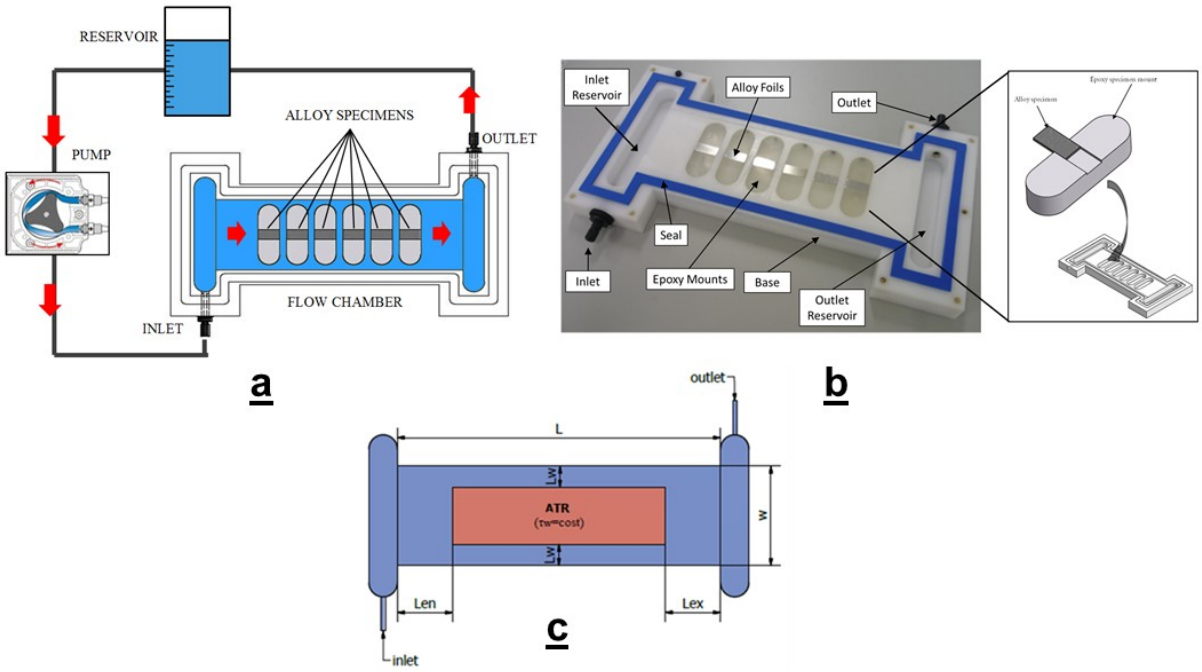

Fig. 1 (a) A schematic of the bioreactor system developed in this work. (b) A labelled diagram of the parallel plate flow chamber, with the use of epoxy mounts shown in the outset. (c) A schematic of the active test region (ATR) and important dimensions for the flow chamber.

An annotated image of the PPFC is shown in Fig. 1 (b). The PPFC consists of an acetal base with an inlet and outlet reservoir. Between the reservoirs there is a parallel plate region of cuboidal geometry with depth h, width w and length L. Six slots are cut in the base into which epoxy resin mounts can be placed. The use of the mounts allows alloy samples with different geometries to be studied, while ensuring a flush surface in the parallel plate region. A transparent poly-methyl-methacrylate (PMMA) lid is placed over the base to facilitate visualization of alloy samples and flow patterns during tests. The chamber is sealed using a rubber foam gasket. Fig. 1 (c) shows the dimensions of importance for the PPFC and the ATR. Dimensions that satisfy the previously listed requirements for the chamber are determined using analytical methods and CFD.

In designing the flow chamber a constant flow is assumed in place of the pulsatile flow present in the actual system. As such, in the following analysis quantities are assumed to have values averaged over a cycle in the flow. The flow rate Q required to give a WSS, τ_w, between

1.5 and 2.0 Pa for a fluid with viscosity μ is found from the following expression for fully developed flow between two infinite parallel plates:[11]

$$\tau_w = \frac{6\mu Q}{w h^2} \tag{1}$$

To investigate if the effects of lateral walls (i.e. finite channel width) lead to a varying WSS across the ATR, the following expression for fully developed flow through a rectangular duct is used to find the change in WSS along the channel width:

$$\tau_w(\tilde{y}) = \frac{6\mu Q}{w h^2} \times F(\tilde{y}) = \frac{6\mu Q}{w h^2} \times \frac{1 - \frac{8}{\pi^2} \sum_{n=1,3,5,\ldots}^{\infty} \frac{1}{n^2} \frac{\cosh\left(\frac{n\pi \tilde{y}}{\beta}\right)}{\cosh\left(\frac{n\pi w}{2\beta}\right)}}{1 - \frac{192}{\pi^5} \frac{h}{w} \sum_{n=1,3,5,\ldots}^{\infty} \frac{1}{n^5} \tanh\left(\frac{n\pi}{2\beta}\right)} \tag{2}$$

This expression is derived from the Navier-Stokes equations for steady, uniform laminar flow of an incompressible fluid.[12] In Eqn. 2, $\beta = h/w$, y is the distance to the centre of the chamber (see Fig. 2) and $\tilde{y} = 2y/w$.

Eqn. 2 assumes fully developed flow and does not give a prediction of boundary layer effects near the lateral walls. While analytical models for predicting entrance and exit lengths (L_{en} and L_{ex} in Fig. 1 (c)) and boundary layer width (L_W) exist, due to the complexity of the flow in the vicinity of the input and output reservoirs in the PPFC, CFD is used to investigate boundary layer effects and to determine suitable entrance and exits lengths.

In designing the PPFC a WSS of 2 Pa in the ATR is sought. Based on incubator space and microscopy requirements, a width of 70 mm and channel height of 0.25 mm are chosen. Assuming a density ρ of 993 kg m^{-3} and viscosity of 0.0007 Pa s for the test media being used, which correspond to the values for water at 37 °C, the required flow rate is found to be

125 ml min^{-1}, based on the application of Eqn 1. While the viscosity of the actual test media used may differ from that of water, for Hank's balanced salt solution and Dulbecco's modified Eagle's medium the increase in viscosity is expected to be less than 5% over that of water, even with the addition of up to 10% serum.[13,14] For these dimensions and assumptions the mean velocity $\acute{v}$ in the rectangular channel is:

$$\acute{v} = \frac{Q}{wh} = \frac{125\,\text{ml min}^{-1}}{70\,\text{mm} \times 0.25\,\text{mm}} \approx 0.12\,\text{m s}^{-1} \tag{3}$$

while the Reynolds number is:

$$\Re = \frac{\rho \acute{v} h}{\mu} = \frac{993\,\text{kg m}^{-3} \times 0.12\,\text{m s}^{-1} \times 0.25\,\text{mm}}{0.0007\,\text{Pa s}} = 42.2 \tag{4}$$

suggesting a laminar flow. The effects of lateral walls on the shear stress along the channel width is found to be minimal, by applying Eqn. 2, with a plot of the correction factor $F(\tilde{y})$ across the channel width shown in Fig. 2.

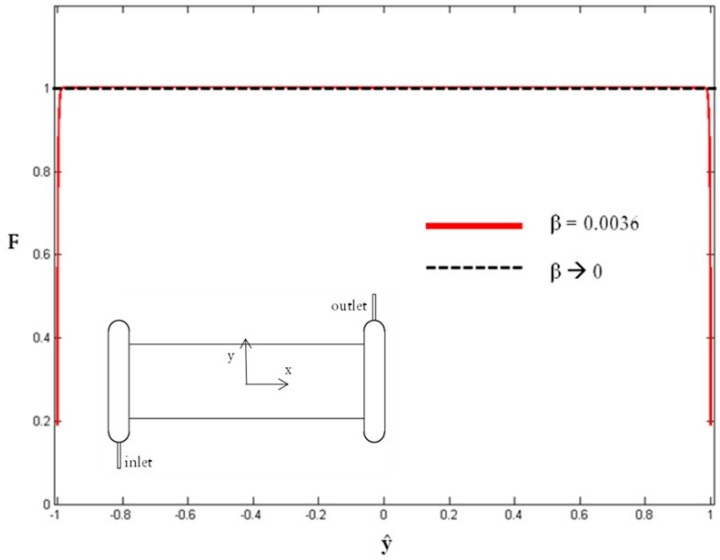

Fig. 2 A plot of the correction factor F in Eqn. 2 with normalized distance to the centre of the flow chamber. For the chamber dimensions used in this study the lateral walls are found to have a

negligible effect of wall shear stresses. $\beta = h/w$, where h is the depth and w the width of the flow chamber.

CFD analysis of the PPFC is performed using ANSYS Fluent (version 12.1, ANSYS Inc., United States). The computational domain is shown in Fig. 3. For the mesh, hexahedral elements (8 nodes) are used for the channel region and inlet and outlet tubes, while tetrahedral elements are used for the reservoirs. Overall, the mesh consists of 843,669 elements. The velocity at the inlet port is:

$$v_{¿} = \frac{Q}{\pi\left(\frac{D}{2}\right)^2} = \frac{125\,\text{ml min}^{-1}}{\pi\left(\frac{3\,\text{mm}}{2}\right)^2} \approx 0.295\,\text{m s}^{-1} \quad (5)$$

where D is diameter of the tubular inlet. $v_{¿}$ is applied as a velocity boundary condition at the inlet port in the CFD analysis. A zero pressure is set as a boundary condition at the outlet, while no-slip is assumed on all walls. The analysis assumes time independent flow conditions. Based on the results of the CFD analysis an overall channel length of 228 mm is chosen, which ensures: i) sufficient entrance and exit lengths of 39 mm each, ii) enough room to fit all six sample slots and iii) a suitable overall length to allow the chamber to fit in an incubator. It is also verified that the total chamber width of 70 mm is sufficient to account for boundary layer effects at the lateral walls, by taking L_w as 15 mm.

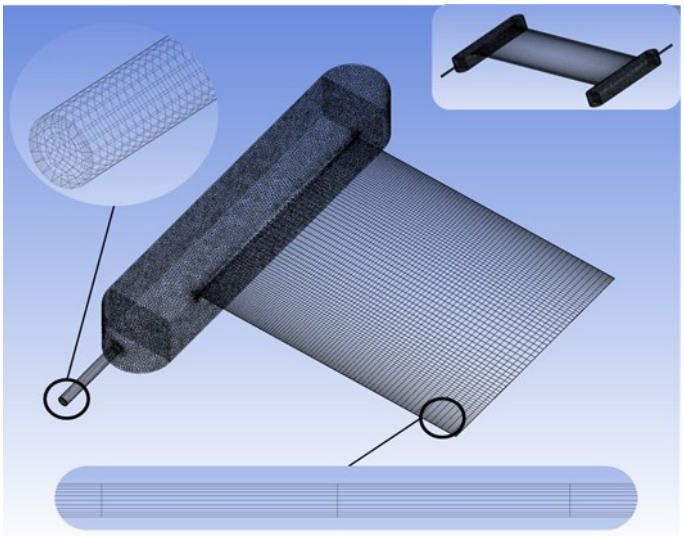

Fig. 3 Half of the computation domain used to analyse the PPFC. The full computational domain is shown in the inset at the top-right. The other insets show details of the mesh in the inlet tube (top-left) and the layer through the channel height (bottom) containing ten elements.

2.2 AZ31 Corrosion Study

The bioreactor is used to evaluate the corrosion rate of the alloy AZ31 (Goodfellow Ltd., UK) in pseudo-physiological dynamic flow conditions. Foil corrosion in static solutions is also investigated, with samples with a single exposed surface held in beakers in this case. Foil samples with thicknesses of 0.25 mm and 1.0 mm are used. For static tests foils are cut into 10 mm x 10 mm samples, while for dynamic tests they are cut into 20 mm x 10 mm samples. Each sample is prepared by polishing with P1200 emery paper and cleaning in anhydrous ethanol. Specimen mass is determined using a mass balance with a resolution of 0.1 mg. Before determining the mass loss, specimens are cleaned in heated chromic acid to remove corrosion products deposited on the surface.

Three different media are used in the corrosion tests, modified Hank's balanced salts solution (HBSS) (cat. no. H1387, Sigma–Aldrich, USA), Endothelial Cell Growth Medium (P-ECGM) (cat. no. C-22020, Promocell, Germany) and Dulbecco's modified Eagle's medium (D-MEM) (cat. no. d5796, Sigma-Aldrich, USA) supplemented with 10% foetal bovine serum (FBS). HBSS is chosen as it has been widely employed as a pseudo physiological solution in corrosion tests of biodegradable alloys.[8] HBSS consists of inorganic ions with concentrations generally similar to those in body plasma. However, it has a lower concentration of HCO_3^- (4.0 mmol l^{-1}) than human blood plasma (27.0 mmol l^{-1}).[8] Moreover, HBSS does not contain proteins or amino acids. On the other hand, D-MEM + 10% FBS and P-ECGM (which includes 5 % foetal calf serum) contain both organic ions and inorganic ions, including amino acids, vitamins and proteins, such as in blood serum. The protein concentrations used in this study are somewhat less than physiological quantities, but are typical of amounts used in cell culture. These testing media are therefore chosen to assess the

influence of proteins and amino acids on the alloy corrosion behaviour and in order to obtain more corrosion rates that are more representative of those observed *in-vivo*. The solution volume (ml) to surface area (cm^2) ratio is maintained between 10:1 and 46:1 in all tests, with this range being deemed appropriate based on the work of Yang and Zhang,[14] who showed that increasing the volume to area ratio beyond 6.7 had little influence on the corrosion behavior of a similar biodegradable magnesium alloy in HBSS.

Immersion tests are performed both in a static environment (no flow) and dynamic environment (with flow), with the peristaltic pump delivering a flow rate of 125 ml min^{-1}, as decided based on the analysis of the previous section. The duration of the tests (up to 140 hours) reflects approximately the amount of time required for the build-up of a neo-intimal layer in vascular applications.[15] Since this layer, which may form a barrier between the corrosion surface and the flow, is not accounted for in these immersion tests a higher corrosion rate than would be observed *in-vivo* is expected. A more representative physiological environment, including an endothelial layer, is attainable using the developed bioreactor and would allow the assessment of longer-term corrosion rates, but is not considered in this study. Cell culture conditions, i.e. buffering of the culture media and the use of a controlled CO_2 environment, are not used in the experimental portion of the study, however the system is designed to facilitate such conditions through the use of an open reservoir, Tygon tubing for gaseous exchange and the sizing of the system to fit in an incubator with a controlled environment.

3. Results and Discussion

3.1 CFD Analysis

Fig. 4 (a) shows a plot of the predicted WSS in the PPFC from the CFD analysis. It shows that the WSS is constant and uniform in the ATR. The value of the WSS, $\tau_w \approx 1.9$ Pa, inside

the ATR is confirmed to be within the desired physiological range of $1.5 < \tau_w < 2.0$ Pa. Figs. 4 (b) and 4 (c) show WSS profiles on important planes in the PPFC. A drop in WSS toward the centre of the planes in the entrance and exit regions is noted, however WSS is constant along planes in the ATR. Fig. 4 (d) shows path-lines in the flow coloured by velocity magnitude. Based on this, flow is expected to be laminar in the ATR. This analysis confirms that the chosen design maintains suitable flow conditions on the exposed surfaces of alloy samples and also allows for an accurate quantification of mean WSS (1.9 Pa) in the ATR. As can be seen from Figs. 2, 4 (b) and 4 (c) there is predicted to be very little influence of boundary and entrance effects on flow in the ATR for the averaged velocity over a cycle of the pulsatile flow. Based on this, it is assumed that the influence of these effects over the course of a cycle in the pulsatile flow in the actual PPFC is also negligible.

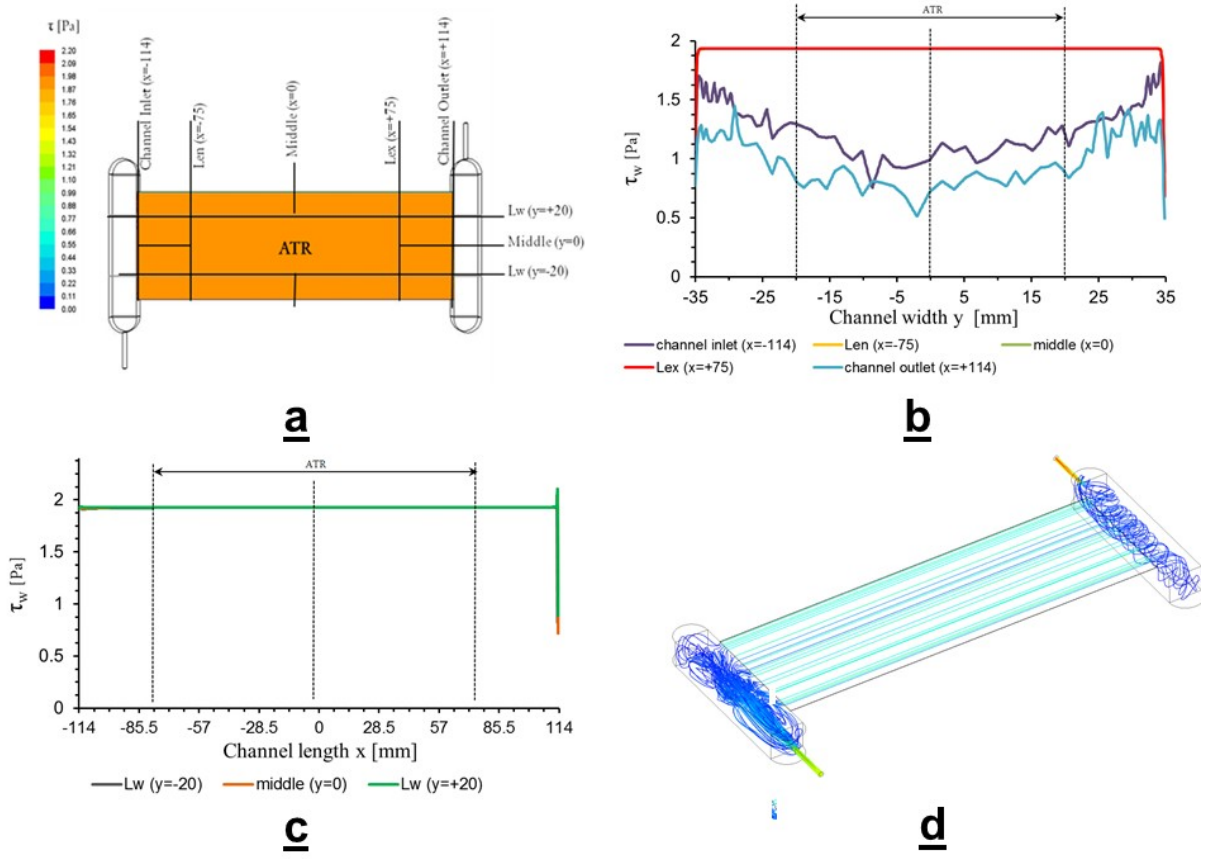

Fig. 4 (a) Contours plot of the wall shear stress at the channel bottom wall. Section planes where wall shear stresses are evaluated for the plots in (b) and (c) are also indicated, according to the coordinate

system in Fig. 2. (b) WSS evaluated at the section planes along the width (y) of the channel. (c) WSS evaluated at the section planes along the length (x) of the channel. (d) Predicted flow path-lines in the chamber coloured by velocity magnitude.

3.2 AZ31 Corrosion Study

Fig. 5 (a) compares mass loss in static HBSS and P-ECGM for foils of 0.25 mm thickness. The mass loss rate (based on the final time point) is higher in the HBSS (0.174 mg cm^{-2} h^{-1}) than in the cell culture media (0.048 mg cm^{-2} h^{-1}). Fig. 5 (b) compares mass loss in 1.0 mm thick foils in static HBSS and D-MEM. The mass loss rate in the HBSS (0.05 mg cm^{-2} h^{-1}) is higher than in the D-MEM (0.0148 mg cm^{-2} h^{-1}). The change in pH for the points shown in Fig. 5 (b) is shown in Table 1. There is an initial increase in pH in both media, from 6.7 to 8.2 and 7.4 to 8.0 in the HBSS and D-MEM respectively. The pH in the HBSS remains constant for the remainder of the test, while there is a slight drop in the pH of the D-MEM.

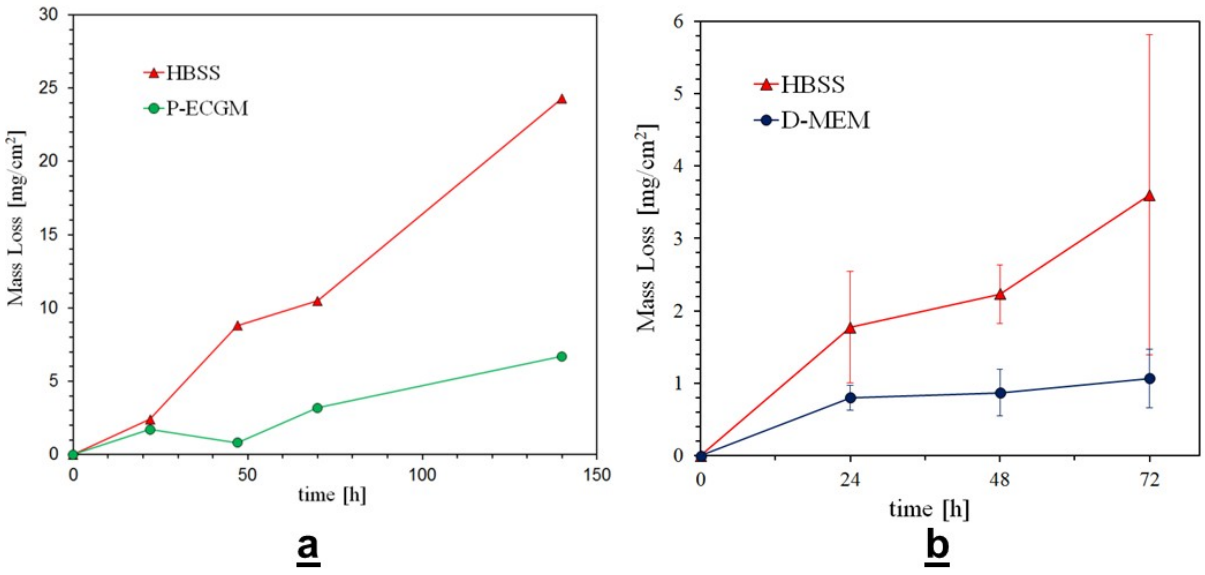

Fig. 5 Mass loss in (a) 0.25 mm thick AZ31 foils immersed in static HBSS and P-ECGM (n = 1) and (b) 1.0 mm thick AZ31 alloy foils immersed in static HBSS (n = 3) and D-MEM (n = 5).

Fig. 6 shows the degradation of foils in static HBSS, P-ECGM and D-MEM. Under macroscopic observation, the corrosion surfaces of the foils in HBSS are characterised by the growth and coalescence of a number of large corrosion pits, as shown in Fig. 6 (a). Under microscopic observation (SEM), the surface is characterised by a combination of large pits

(Fig. 7 (a)) and regions of localized corrosion spread through the remainder of the surface (Fig. 7 (b)). For foils in P-ECGM, the corrosion surface is characterized by the growth of a small number of large corrosion pits (Fig. 6(a)). Under SEM the corrosion surface contains some pits (Fig. 7 (c)), but is mostly comprised of regions with little or no localized corrosion (Fig. 7 (d)). For foils in static D-MEM, the corrosion surface contains no noticeable macroscopic pits (Fig. 6 (b)), but under SEM the corrosion surface is observed to consist of mostly regions with small amounts of localized corrosion (Location 1 in Fig. 8), with larger hemi-spherical pits also developing in some regions (Location 2 in Fig. 8).

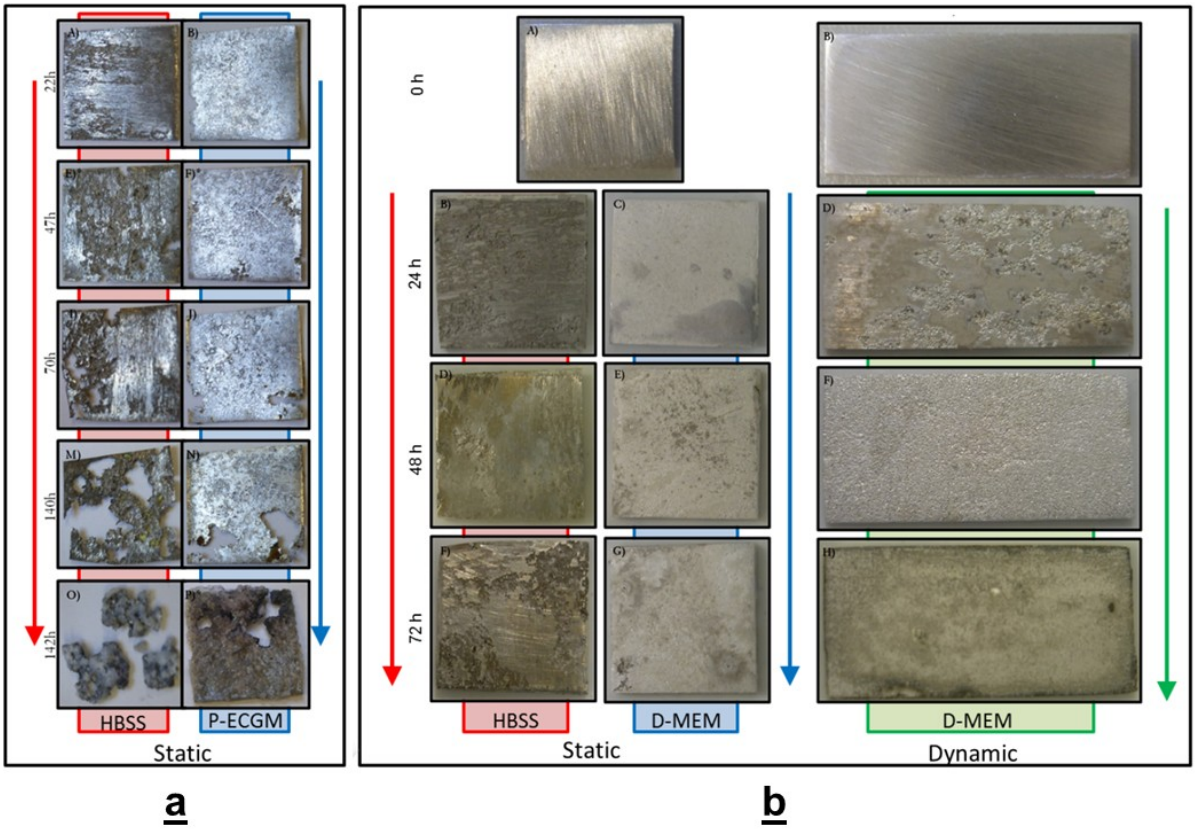

Fig. 6 Images of corroded and cleaned AZ31 alloy foils in static and dynamic conditions. Foils in (a) have thickness 0.25 mm and foils in (b) have thickness 1.0 mm.

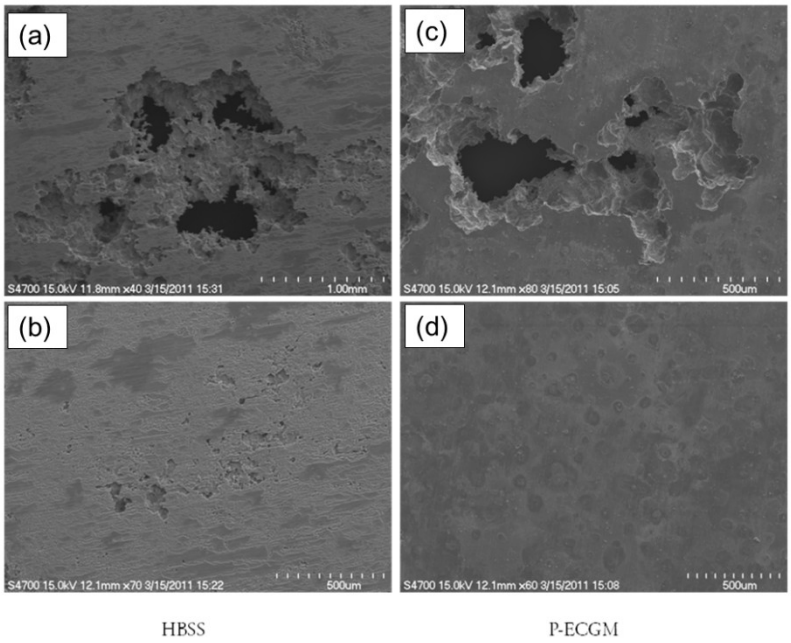

Fig. 7 SEM images of 0.25 mm thick foils immersed in HBSS (a and b) and P-ECGM (c and d) for 47 hours.

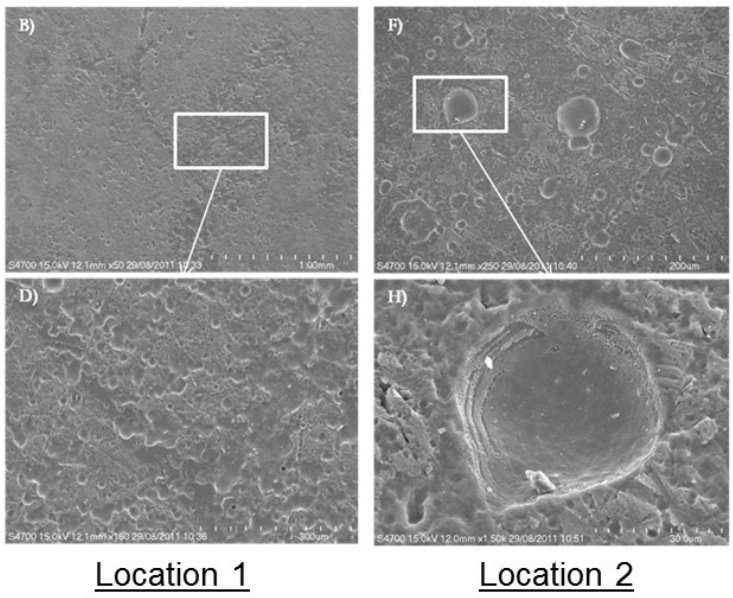

Fig. 8 SEM images of 1.0 mm thick foils immersed in static solutions of D-MEM for 72 hours.

The relatively high corrosion rate and pitting severity observed for foils in HBSS may be due to a combination of: i) the lack of proteins, which were included in the P-ECGM and D-MEM, ii) the higher content of Cl^- ions in HBSS (145 mmol l^{-1}) than in D-MEM (91 mmol l^{-1}) and in human blood plasma (103 mmol l^{-1}) and iii) the lower content of $HCO3^-$ ions in HBSS (4.2 mmol l^{-1}) compared to D-MEM (44 mmol l^{-1}) and human blood plasma (27 mmol

l^{-1}).[8] It has been reported that protein adsorption onto the magnesium surface significantly reduces corrosion rates.[16,17] This may be attributed to the tendency of adsorbed proteins to encourage the formation of an insoluble salt layer, making an effective barrier against corrosion. Chlorine ions are known to speed up corrosion and encourage pitting behavior, while $HCO3^-$ ions are known to reduce corrosion rates by facilitating the build-up of a protective layer of corrosion product.[8]

Based on these observations, D-MEM appears to be the most suitable choice of pseudo-physiological media for the bioreactor, due to the relatively low corrosion rate of the AZ31 alloy in this media, which is more representative of *in-vivo* observations of corrosion rates, and the ability, with some additions, to be used for cell culture.

Fig. 9 (a) compares mass loss in static HBSS for foils of thickness 0.25 and 1.0 mm. The mass loss rate is higher in the thinner foils (0.174 mg cm^{-2} h^{-1}) than the thicker (0.050 mg cm^{-2} h^{-1}). This difference in corrosion rates may be explained with reference to Fig. 6. Fig. 6 (a) shows the degradation of 0.25 mm thick foils in HBSS, with a large number of corrosion pits growing through the foil thickness and then spreading laterally. For the thicker foils however, shown in Fig. 6 (b), pits do not pass through the foil thickness, and as a result less surface area is exposed and there is a greater chance for corrosion-product accumulation. This different corrosion behaviour with different foil thickness is an important geometrical consideration for such tests, especially given that magnesium stent struts have dimensions on the order of 0.1 to 0.15 mm.

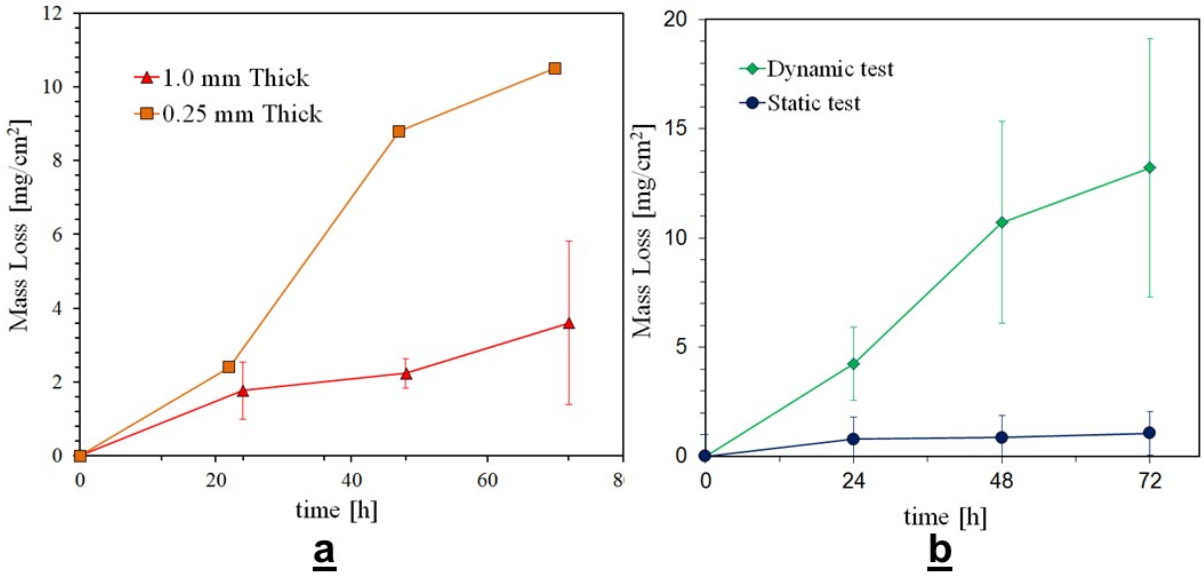

Fig. 9 Mass loss in (a) 0.25 mm (n = 1) and 1.0 mm (n = 3) thick AZ31 foils immersed in static HBSS and (b) 1.0 mm thick AZ31 foils in static and dynamic D-MEM (n = 5).

Fig. 9 (b) compares mass loss for 1.0 mm thick foils in static and dynamic D-MEM, with the change in pH shown in Table 1. The mass loss rate in the dynamic tests (0.184 mg cm^{-2} h^{-1}) is considerably higher than in the static (0.0148 mg cm^{-2} h^{-1}). For foils in static D-MEM it was reported earlier that on macroscopic observation no pitting was observed. For samples in flowing D-MEM however, localized corrosion was observed to begin in certain regions, consisting of a large number of small corrosion pits, and eventually cover the entire sample surface, as shown in Fig. 6 (b). Under SEM, the pits in the regions undergoing localized corrosion are initially hemispherical and have a smoothed appearance (see Fig. 10), relative to those in Fig. 8. As corrosion progresses in the flowing solution, a number of different morphologies arise, as shown in Fig. 10. After 72 hours of immersion there is evidence of undermining and also preferential corrosion around certain regions, which remain protruding from the corrosion surface.

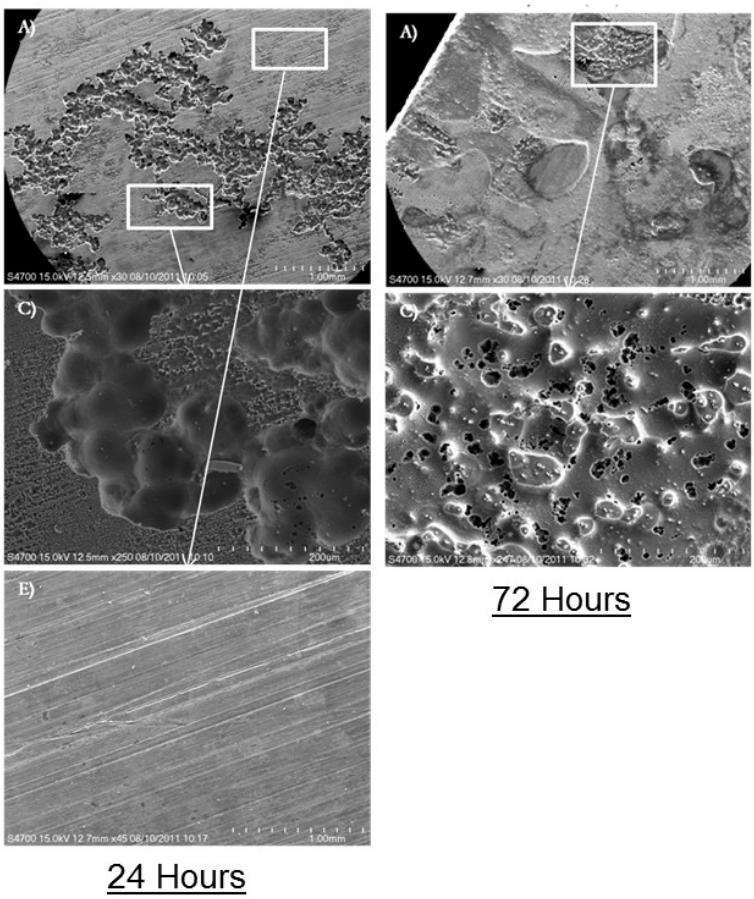

Fig. 10 SEM images of 1.0 mm thick foils immersed in dynamic solutions of D-MEM for 24 and 72 hours.

In the dynamic corrosion tests, mass loss is significantly increased when compared to static immersion tests in the same media (D-MEM + FBS) at all time points. Fluid flow thus has a significant impact on corrosion behavior and should be accounted for in order to obtain realistic corrosion rates of biodegradable alloys. It is noted that the increase in corrosion rate may be ascribed to both the presence of a shear stress at the corrosion surface and also the increased media volume and exchange rate in the flowing relative to static media. According to SEM micrographs, pits observed on the specimen in the dynamic corrosion test (Fig. 10) seem to be smoothed out to a certain degree, when compared to the pits observed on the surface of the static sample (Fig. 8). This could be ascribed to fluid flow.

A comparison of the corrosion rates obtained in this study with those of other *in-vitro* and *in-vivo* studies is given in Table 2. Observed corrosion rates for 1.0 mm AZ31 foils are within

the range of those reported for 2.0 – 2.5 mm foils in static HBSS.[18] The observed increase in corrosion rate for AZ31 in flowing D-MEM relative to static is in agreement with observations for pure Mg and WE43 alloy in static and flowing HBSS.[19] The observed static corrosion rate for 1.0 mm D-MEM foils is in agreement with observations for 3.0 mm foils in MEM with serum albumin.[20] The corrosion rates observed in both static and flowing media are higher than those observed in *in-vivo* subcutaneous tests on AZ31 samples, [20] with the rate from the flow tests being significantly higher. This suggests that the effect of tissue surrounding the implant has an important influence on corrosion rate and that including the effects of flow alone may not sufficiently capture the physiological corrosion environment.

An important follow-on to the study presented here is the culturing of cells within the developed bioreactor. This would give many useful insights into the ability of tissue layers on the biodegradable alloy to counteract the increased corrosion rate due to transport conditions in the dynamic fluid.

4. Conclusions

The goal of this study was the development of a bioreactor system to replicate the *in-vivo* corrosion environment as closely as possible. Through the use of analytical methods and computational fluid dynamics, a bioreactor that could theoretically be used to cultivate cells and also study the corrosion of biodegradable metals in a dynamic solution was developed. The bioreactor was used to study the corrosion of AZ31 alloy foils of different thickness, in different media and with static and dynamic conditions.

Different corrosion behaviours were observed in foils of different thickness, with the thinner foils having a higher corrosion rate and greater susceptibility to large pit growth. This finding may be of importance when the dimensions of stent struts are considered. Foils corroded more quickly and with more pitting in Hank's balanced salt solution (HBSS) than other

media, which is attributed to the lack of proteins, greater chlorine content and lower hydrogen carbonate content in HBSS than in the other media. It is concluded that Dulbecco's modified Eagle's media is the most suitable solution for use in the bioreactor.

Pulsatile flow conditions significantly increased corrosion rates relative to static tests and led to localized corrosion with smoothed hemispherical pits. It is concluded that fluid flow is an important consideration when assessing the performance of candidate biodegradable alloys, both in terms of corrosion rates and corrosion surface morphology.

Acknowledgements

The authors would like to acknowledge funding from the Irish Research Council under the Embark Initiative (J. A. Grogan) and from the Fondazione Cassa di Risparmio di Trento e Rovereto (F. Migliavacca and D. Gastaldi). Mr William Brennan and Mr Dermot Daly are also acknowledged for their help in the manufacture of the flow chamber.

References

[1]A.T.L. Ong, E.P. McFadden, E. Regar, P.P.T. De Jaegere, R.T. Van Domburg and P.W. Serruys, J. Am. Coll. Cardiol. **45**, 2088 (2005).

[2]A.K. Mitra and D.K. Agrawal, J. Clin. Pathol. **59**, 232 (2006).

[3]M.P. Staiger, A.M. Pietak, J. Huadmai and G. Dias, Biomaterials **27**, 1728 (2006).

[4]R. Erbel, C. Di Mario, J. Bartunek, J. Bonnier, B. De Bruyne, F.R. Eberli, P. Erne, et al., Lancet **369**, 1869 (2007).

[5]F. Witte, N. Hort, C. Vogt, S. Cohen, K.U. Kainer, R. Willumeit and F. Feyerabend, Cur. Opin. Solid State Mater. Sci. **12**, 63 (2008).

[6]N.T. Kirkland, J. Lespagnol, N. Birbilis and M.P. Staiger, Corros. Sci. **52**, 287 (2010).

[7]R. Willumeit, J. Fischer, F. Feyerabend, N. Hort, U. Bismayer, S. Heidrich and B. Mihailova, Acta Biomater. **7**, 2704 (2011).

[8]Y. Xin, T. Hu and P.K. Chu, Acta Biomater. **7**, 1452 (2011).

[9]B. Chung, A. Robertson and D. Peters, Comput. Struct. **81**, 535 (2003).

[10]A.M. Malek, J. Amer. Med. Assoc. **282**, 2035 (1999).

[11]F. White, *Fluid Mechanics* (McGraw-Hill, USA, 2006).

[12]R. Berker, in *Handbuch der Physik, vol. VVIII/2,* edited by C. Truesdell (Springer-Verlag, Berlin, 1963), pp. 70–71.

[13]G.J. Medema, F.M.., Schets, F. M. and P.F.M. Teunis, Appl. Environ. Microbiol. **64**, 4460 (1998).

[14]P.M. Hinderliter, K.R. Minard, G. Orr, W.B. Chrisler, B.D. Thrall, J.G. Pounds and J.G. Teeguarden, Part. Fibre Toxicol. **7**, 36 (2010).

[14]L. Yang and E. Zhang, Mater. Sci. Eng. C **29**, 1691 (2009).

[15]C. Di Mario, H. Griffiths, O. Goktekin, N. Peeters, J. Verbist, M. Bosiers and R. Erbel, J. Interv. Cardiol., **17**, 391 (2004).

[16]A. Yamamoto and S. Hiromoto, Mater. Sci. Eng. C **29**, 1559 (2009).

[17]Y. Wang, C.S. Lim, C.V. Lim, M.S. Yong, E.K. Teo and L.N. Moh, Mater. Sci. Eng. C **31**, 579 (2011).

[18]H. Wang, Y. Estrin, H. Fu, G. Song and Z. Zúberová, Adv. Eng. Mater. **9**, 967.

[19]N. Li, C. Guo, Y.H. Wu, Y.F. Zheng and L.Q. Ruan, Corros. Eng. Sci. Technol. **47**, 6 (2012).

[20]J. Walker, S. Shadanbaz, N.T. Kirkland, E. Stace, T. Woodfield, M.P. Staiger and G.J. Dias, J. Biomed. Mater. Res. B **100**, 1134 (2012).

Table 1 pH values for the static immersion tests on HBSS and D-MEM. pH values taken from the reservoir of the flow chamber for the flow tests on D-MEM samples are also included.

Time (hrs)	HBSS, Static	D-MEM, Static	D-MEM, Flow
0	6.70	7.40	7.4
24	8.24 ± 0.28	7.97 ± 0.30	8.28
48	8.18 ± 0.17	7.83 ± 0.04	6.07
72	8.04 ± 0.32	7.58 ± 0.01	7.12

Table 2 A comparison of corrosion rates measured in this study and those from the literature for samples tested in static and flowing media and *in-vivo*.

Sample	Media	Flow	Corrosion Rate ($mg\ cm^{-2}\ hr^{-1}$)	Source
AZ31 (0.25 mm foil)	HBSS	No	0.174	Fig. 9 (a)
AZ31 (1.0 mm foil)	HBSS	No	0.05	Fig. 9 (a)
AZ31 (1.0 mm foil)	D-MEM	No	0.015	Fig. 9 (b)
AZ31 (1.0 mm foil)	D-MEM	Yes	0.184	Fig. 9 (b)
AZ31 (2.0 – 2.5 mm foil)	HBSS	No	0.033 – 0.088	[18]
Pure Mg (rod)	HBSS	No	0.182	[19]
Pure Mg (rod)	HBSS	Yes	0.626	[19]
AZ31 (3.0 mm plate)	MEM with serum albumin	No	0.019 – 0.039	[20]
AZ31 (3.0 mm plate)	*In-vivo*	NA	0.004 – 0.007	[20]